Power Plant Steels: Remanent Life Assessment and the Approach to Equilibrium

H. K. D. H. Bhadeshia
University of Cambridge
Department of Materials Science and Metallurgy
Pembroke Street, Cambridge CB2 3QZ, U. K. hkdb@cus.cam.ac.uk

ABSTRACT

The steels used in the power generation industry are almost always given a severe tempering heat–treatment before they enter service. This would, in most contexts, give them a highly stable microstructure which is close to equilibrium. In fact, they undergo many changes over long periods of time. This paper is a review of some of the methods which exploit the changes in order to estimate the life that remains in alloys which are only partly exhausted.

INTRODUCTION

Many of the safety–critical components in power plant are made of steels developed to resist deformation when used in the range 480–565 °C and 15–90 MPa. They are expected to serve reliably for a period of about 30 years, giving a maximum tolerable creep strain rate of about $3 \times 10^{-11}\,\mathrm{s}^{-1}$ (approximately 2% elongation over the 30 years). The design stress must be set to be small enough to prevent creep rupture over the intended life of the plant.

The steels are able to survive for such long periods because the operating temperature is only about half of the absolute melting temperature, making the migration of atoms very slow indeed. Creep therefore depends on the ability of dislocations to overcome obstacles with the help of thermal energy. The obstacles are mainly carbide particles which are dispersed throughout the microstructure.

Suppose that the microstructure and the operating conditions do not change during service. The accuracy with which component life might then be predicted would depend only on the quality of the experimental data. The so–called "safety factors" common in design could then be greatly reduced with obvious benefits. Of course, this never happens in practice; the steels are always heterogeneous and the service conditions vary over a range of scales and locations. The design life is therefore set conservatively to account for the fact that measured creep data follow a Gaussian distribution with a significant width. In spite of this, experience has shown that decommissioned plant could have been kept in service without sacrificing safety. To take advantage of this observation requires methods for the reliable estimation of the *remaining life*. The techniques used for this purpose are summarised in Table 1. Of the properties listed, no single measurement is comprehensive enough to describe the steel with all requisite completeness. The implementation of a life–extension procedure must consequently be based on broad considerations backed by more frequent inspections.

DAMAGE SUMMATION

A satisfactory way of representing creep damage (C) is to use a parameter (ω) which is normalised by its value at failure (ω_r). The magnitude of ω_r will depend on the precise values of stress (σ), temperature (T) and any other variable which influences the creep process. Since these variables are not necessarily constant, the extent of damage is often written [1,9]

$$C = \sum_i \frac{\omega_i}{(\omega_r)_i} \tag{1}$$

Property	Example references
Damage summation	Evans, 1984 [1]
Hardness	Goto, 1984 [2]
Tensile test	Cane and Williams, 1987 [3]
Interparticle spacing	Askins and Menzies, 1985 [4]
Cavitation parameter	Gooch *et al.*, 1989 [5]
Number density of cavities	Dyson and McLean, 1972 [6]
Fraction of cavities	Walker and Evans [7]
Impact toughness	Wignarajah *et al.* [8]

Table 1: Some of the methods used in the estimation of remaining life.

ω is typically the time or the creep strain. Failure occurs when the sum achieves a value of unity.

Evans [1] argues that it is more appropriate to use the strain rather than the time, since the latter is not considered as a "state variable". In the context of thermodynammics, the state of a system can in principal be specified completely by a number of state variables (such as temperature, pressure) such that its properties do not depend at all on the path by which those variables were achieved. This clearly cannot be the case even for the creep strain. This is because the extent of damage *is* expected to depend on the path by which a given value of strain is achieved, for example, whether the strain is localised at grain boundaries or uniformly distributed. This necessarily means that equation 1 is an approximation; as Evans states, it should be a reasonable approximation if the mechanism of creep does not change between the components of the summation. Thus, Cane and Townsend [10] conclude that the use of the life fraction rule in taking account of temperature variations is more justified than for variations in stress. This is because for the latter case, the dislocation networks become finer (relative to the carbide spacings) at large stresses. The network nodes then do not coincide with carbide particles, thus changing the mechanism of deformation. This is not the case with variations in temperature because the dislocation network then scales with the particle spacing. The failure of the life fraction rule is sometimes accommodated by empirically setting the limiting value of C to some positive value which is not unity.

HARDNESS, INTERPARTICLE SPACING

The hardness can be used as an indicator for the state of the steel in its life cycle. Changes in hardness occur due to recovery, coarsening of carbide particles, and recrystallisation. All creep–resistant power plant steels are severely tempered before they enter service. They are therefore beyond the state where secondary hardening is expected and the hardness can, during service, be expected to decrease monotonically. In these circumstances, an Avrami equation adequately represents the changes in hardness,

$$\xi = 1 - \exp\{-k_A t^n\} \tag{2}$$

where t is the time, k_A and n rate constants and ξ is given by

$$\xi\{t\} = \frac{H_0 - H\{t\}}{H_0 - H_\infty} \tag{3}$$

where H_0 is the initial hardness, H_∞ is its hardness at the end of useful life and $H\{t\}$ the hardness at time t.

The hardness at the point where the microstructure is exhaustively annealed is likely to be around $H_\infty = 150 - 190$ HV for most power plant steels. Its main components include the intrinsic strength of iron and solid solution strengthening. The starting hardness is likely to be in the range $H_0 = 220 - 300$ HV. Therefore, all that can be expected is a change in hardness of about 30–70 HV over a period of some 30 years. Thus, Roberts and Strang [11] have shown that the hardness can decrease by about 20% in the stressed regions of long–term creep test specimens; this is consistent with an approximately 25% reduction found by Maguire and Gooch [12]. Fig. 1 shows the nature of the changes in hardness to be expected typically, as reported by Maguire and Gooch [12] for a 1CrMoV steel which was tempered at 700 °C for 18 h prior to the ageing at temperatures in the range 600–640 °C.

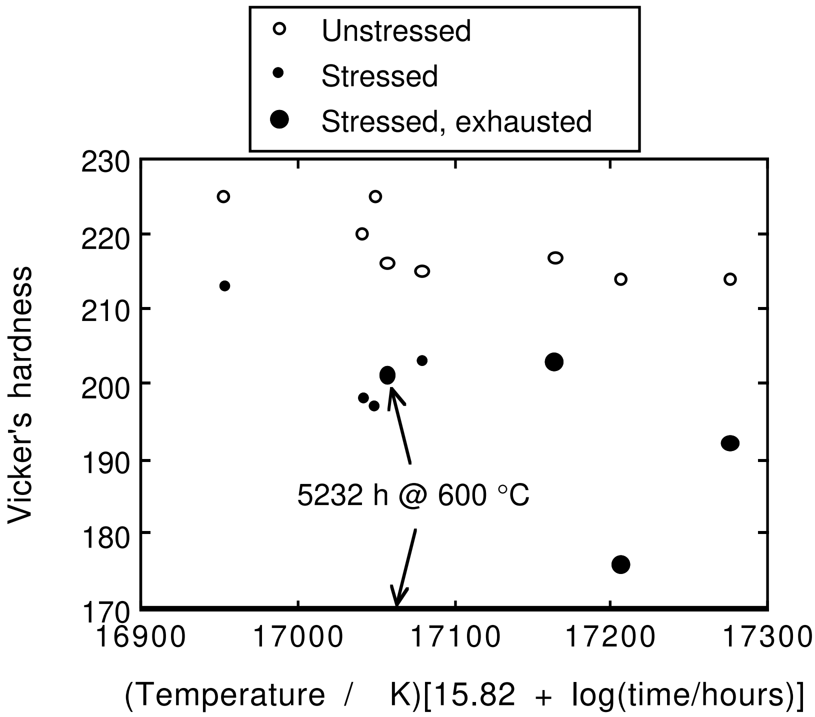

Fig. 1: Changes in the hardness of a 1CrMoV steel during ageing in the temperature range 600–640 $°C$. The samples were tempered at 700 $°C$ for 18 h prior to testing; the effect of the 700 $°C$ treatment is not included in the calculation of the time–temperature parameter plotted on the horizontal axis. The open circles are data from the grips of a creep test specimen, and the filled circles represent measurements from the gauge length. The large filled circles correspond to samples whose hardness values were measured at failure, *i.e.* after the complete exhaustion of life. The stress applied during each of the tests was 93 MPa. Data from Maguire and Gooch.

Precipitates impede the motion of dislocations and any strength in excess of H_∞ is often related to the spacing (λ) between the particles (Cane *et al.*, 1986, 1987):

$$H - H_\infty \propto \frac{1}{\lambda} \propto t^{-\frac{1}{3}} \tag{4}$$

where it is assumed that $\lambda \propto t^{\frac{1}{3}}$ in order to be consistent with coarsening theory.

It is well known that differences in hardness develop in the grip and gauge length of a creep test specimen (Fig. 1). The strain in the gauge length leads to accelerated softening. In fact, the hardness reduction that occurs in the gauge length is roughly proportional to that in the grip [12]. Tack *et al.* [13] have therefore taken H to be a function of strain:

$$\frac{H\{t\} - H\{t,\epsilon\}}{H\{t\} - H_\infty} = b_1 + b_2 \ln\{\epsilon\} \tag{5}$$

where b_1 and b_2 are empirical constants. This illustrates the fact that hardness is a crude indicator of remaining life. Furthermore, it's ability to account for creep damage in the form of voids is not represented in any theory. Hardness tests can therefore only serve a useful purpose in the regime of steady–state creep, before the onset of gross damage. This is evident from Fig. 1 where it is seen that specimens with the same hardness are at different life–fractions. There is a further complication, that the hardness of welded regions is likely to be inhomogeneous even when the welds are made with matching compositions. The potential location of failure is then difficult to identify since creep ductility, creep strength and creep strain may vary with position. The weld metal always has a larger oxide content than the parent steel, and hence has a lower creep ductility. It cannot therefore be assumed that failure will always occur in the softest part of the joint. A harder weld may be needed to ensure the same rupture life as the parent steel (Fig. 2).

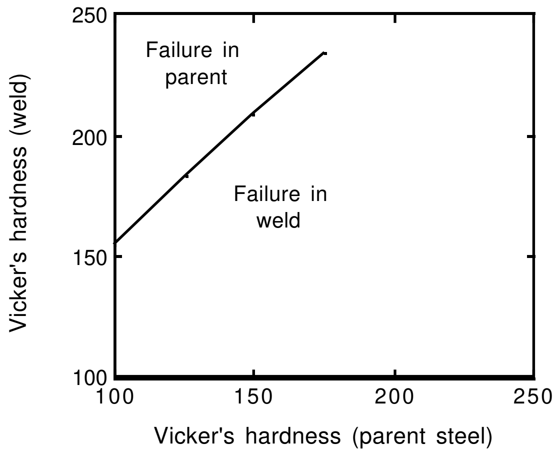

Fig. 2: Data for $2\frac{1}{4}$Cr1Mo steel and matching weld metal. The curve represents the locus of all points along which the weld metal and parent metal have equal rupture lives. Note that for a given life, the weld must be harder than the parent steel (after Tack *et al.*, [13]).

We have seen that hardness can be related inversely to the spacing between precipitate particles; this is illustrated in Fig. 3 for a $1\text{Cr}\frac{1}{2}\text{Mo}$ steel [4]. The spacings are typically measured using transmission electron microscopy at a magnification of about $\times 20,000$ with approximately 100 fields of view covering $30\,\mu\text{m}^2$ taken at random. The actual measurement involves counting the number of particles per unit area (N_A) and it is assumed that $\lambda = N_A^{-\frac{1}{2}}$. The amount of material examined in any transmission microscope experiment is incredibly small, so care has to exercised in choosing representative samples of steel. In some cases, the microstructure may be inherently inhomogeneous. One example is the 12Cr and 9Cr type steels where there is a possibility of regions of δ–ferrite where the precipitation is quite different from the majority tempered martensite microstructure.

Obviously, hardness tests are much simpler to conduct when compared with the effort required to properly measure particle spacings. A further complication is that there is frequently a mixture of many kinds of particles present, some of which continue precipitation during service whereas others dissolve. Thus, Battaini *et al.* [14] found that in a 12CrMoV steel, precipitation continues to such an extent during service that there is a monotonic *decrease* in λ. In fact, the distribution of particles was bimodal with peaks at 30 nm and 300 nm diameters. It is strange that they were only able to correlate the hardness against the changes in the coarser particles. For another steel (12CrMoVW), Battaini *et al.* found an even more complex variation in the interparticle spacing with a maximum value in λ for the coarse particles.

It should be emphasised that the standard error in λ measurements is quite large, frequently larger than the variations observed. Given the difficulties of interpretation, and the experimental error, it is unlikely that λ measurements can be used as a satisfactory general measure of remaining life. The data can nevertheless be of use in the design of physically based creep models.

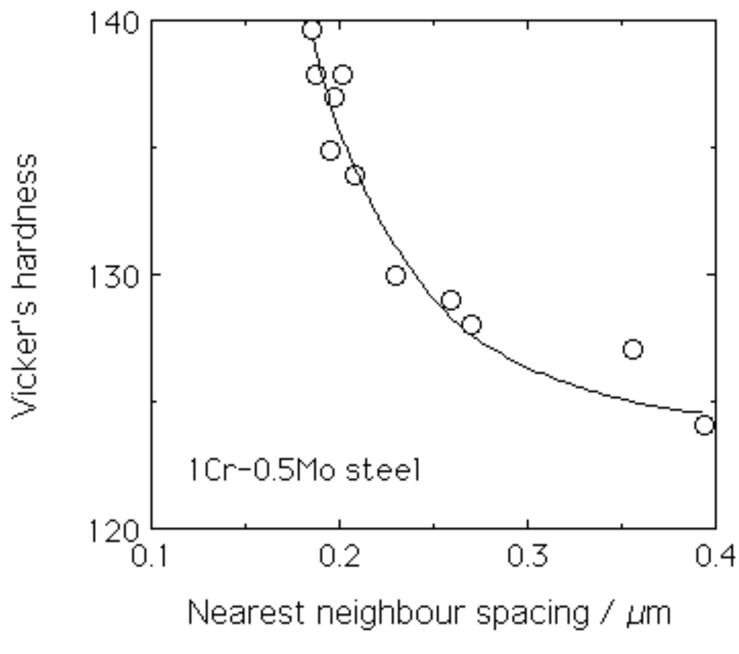

Fig. 3: The hardness as a function of the near neighbour spacing of carbides following creep tests at 630 $^\circ C$ for a variety of time periods. After Askins and Menzies, 1985 [4].

EQUILIBRIUM PHASES

The simplest assumption in kinetic theory is to take a 'flux' to be proportional to the 'force', where the magnitude of the latter depends on the deviation from equilibrium. It follows that to understand the microstructural changes that happen in a steel during service, it is necessary first to consider the equilibrium state. Table 2 lists some of the common power plant alloys together with quotes from material specifications. It seems that the specifications are compiled by agreement between many vested interests and therefore tend to be unrealistically broad. Thus, many of the steels have only a maximum carbon concentration specified! The actual alloys are purchased by users to much tighter ranges than those given in Table 2.

The results of thermodynamic calculations which give the phase fractions and compositions as a function of the overall alloy composition and temperature, are given in Table 3 for the common power plant steels. The calculations have been done using the *MTDATA* computer program and *SGTE* database, taking into account the carbide phases and Laves phase listed. The chemical elements considered are carbon, silicon, manganese, chromium, nickel, molybdenum, vanadium and niobium; nitrogen is not included but is known to be important in forming MX particles. Note also that some very careful work has recently identified an M_5C_2 in 1Cr–0.5Mo steels [15]; this phase has not been included in the analysis.

Designation	M_2X	M_3C	M_7C_3	$M_{23}C_6$	M_6C	Laves	NbC	NbN	VN
$\frac{1}{4}$CrMoV	0.0053			0.0247					
1CrMoV	0.0089			0.0412					
$2\frac{1}{4}$Cr1Mo				0.0335					
Mod. $2\frac{1}{4}$Cr1Mo				0.0211	0.0019				
3.0Cr1.5Mo				0.0185	0.0057				
3.5NiCrMoV	0.0009		0.0161	0.0285					
9Cr1Mo				0.0222					
Mod. 9Cr1Mo				0.0222				0.0009	0.0030
9Cr$\frac{1}{2}$MoWV				0.0248		0.0135		0.0008	0.0032
12CrMoV				0.0443					
12CrMoVW				0.0444		0.0007			
12CrMoVNb				0.0318			0.0006	0.0029	0.0018

Table 3: The mole fractions of precipitate phases in the steels listed in Table 2, when at equilibrium at 565 $^\circ C$ (838 K)

CHANGES IN CARBIDE CHEMICAL COMPOSITIONS

The cementite that forms in association with bainite or martensite has at first, a chemical composition which is far from its equilibrium composition. It therefore enriches with elements such as chromium during service in power plant, and might be used as a built–in recorder for the thermal energy felt by the steel [16–25].

Virgin Cementite

There strong evidence to show that cementite and other iron–based transition carbides grow by a paraequilibrium, displacive transformation mechanism when the precipitation is from martensite or bainite. This subject has been reviewed recently [26]. In this mechanism, the substitutional lattice is displaced into the new structure at a rate controlled by the diffusion of carbon to the transformation front. This is not terribly surprising given the very small distances over which the susbtitutional atoms can diffuse during the precipitation event (Fig. 4). Cementite, for example, precipitates in a matter of seconds during the tempering of martensite.

Designation	C	Si	Mn	Ni	Mo	Cr	V	Others
$\frac{1}{4}$CrMoV	0.15	0.25	0.50	0.05	0.50	0.30	0.25	
range	< 0.18	0.10-0.60	0.40-0.65	–	0.45-0.65	0.25-0.35	0.20-0.30	
1CrMoV	0.25	0.25	0.75	0.70	1.00	1.10	0.35	
range	0.24-0.31	0.17-0.27	0.74-0.81	0.60-0.76	0.65-1.08	0.98-1.15	0.27-0.36	
$2\frac{1}{4}$Cr1Mo	0.15	0.25	0.50	0.10	1.00	2.30	0.00	
range	< 0.16	< 0.5	0.3-0.6	–	0.9-1.1	2.0-2.5	–	
Mod. $2\frac{1}{4}$Cr1Mo	0.1	0.05	0.5	0.16	1.00	2.30	0.25	Ti=0.03 B=0.0024
3.0Cr1.5Mo	0.1	0.2	1.0	0.1	1.5	3.0	0.1	
range	< 0.16	< 0.5	0.30-0.60	–	0.45-0.65	4.0-6.0	–	
3.5NiCrMoV	0.24	0.01	0.20	3.50	0.45	1.70	0.10	
range	< 0.29	< 0.11	0.20-0.60	3.25-4.00	0.25-0.60	1.25-2.00	0.05-0.15	
9Cr1Mo	0.10	0.60	0.40	–	1.00	9.00	–	
range	<0.15	0.25–1.00	0.30–0.60	–	0.90–1.10	8.00–10.00	–	
Mod. 9Cr1Mo	0.1	0.35	0.40	0.05	0.95	8.75	0.22	Nb=0.08 N=0.05
range	0.08–0.12	0.20–0.50	0.30–0.60	<0.2	0.85–1.05	8.00–9.50	0.18–0.25	Nb 0.06–0.10 N 0.03–0.07 Al <0.04
9Cr$\frac{1}{2}$MoWV	0.11	0.04	0.45	0.05	0.50	9.00	0.20	W=1.84 Nb=0.07 N=0.05
range	0.06–0.13	< 0.50	0.30–0.60	< 0.40	0.30–0.60	8.00–9.50	0.15–0.25	Nb 0.03–0.10 N 0.03–0.09 Al <0.04
12CrMoV	0.20	0.25	0.50	0.50	1.00	11.25	0.30	
range	0.17–0.23	<0.5	<1.00	0.30–0.80	0.80–1.20	10.00–12.50	0.25–0.35	
12CrMoVW	0.20	0.25	0.50	0.50	1.00	11.25	0.30	W=0.35
range	0.17–0.23	<0.5	<1.00	0.30–0.80	0.80–1.20	10.00–12.50	0.25–0.35	W<0.70
12CrMoVNb	0.15	0.20	0.80	0.75	0.55	11.50	0.28	Nb 0.30 N 0.06

Table 2: Typical compositions (wt.%) of creep–resistant steels used in the power generation and petrochemical industries. The range of compositions stated lie within the technical specification, but are really intended to reflect the variations observed in practice. The sulphur concentration is usually within the range 0.005–0.02 wt.%, and that of phosphorus within the range 0.005–0.025 wt.%

Of course, not all cementite in power plant steels comes from the bainite or martensite reactions. Many low–alloy steels contain small quantities of pearlite. The cementite which is a constituent of pearlite grows by a reconstructive transformation mechanism in which all of the atoms diffuse in a way which minimises strain energy. But the diffusion at the same time allows

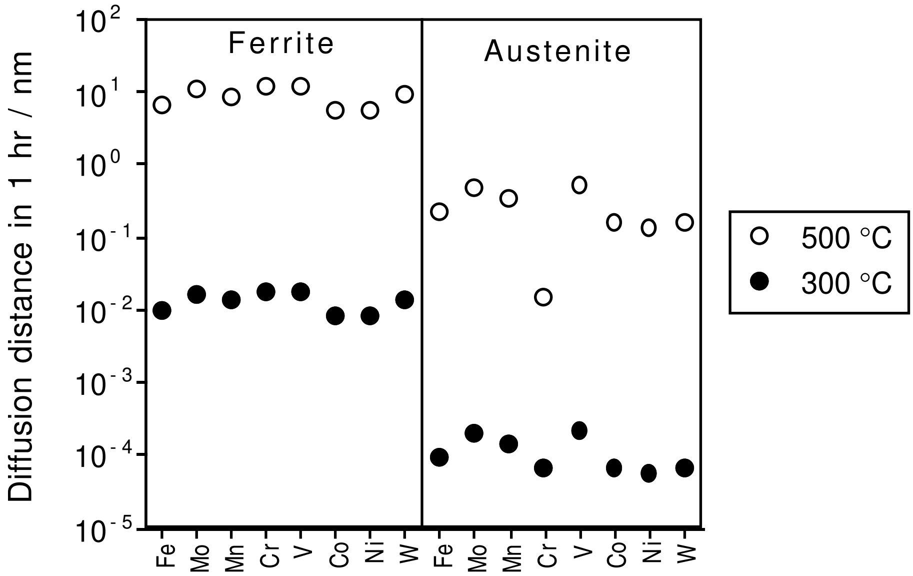

Fig. 4: An illustration of the extraordinarily small diffusion distances at the temperatures where some carbides precipitate.

species of atoms to partition into phases where they are most comfortable. Consequently, the cementite within pearlite always has a chemical composition which is closer to equilibrium. This is illustrated in Fig. 5a, where the cementite when it first forms, is seen to be richer in chromium for pearlite than for bainite. This is the case even when the pearlite and bainite grow at the same temperature [27].

Naturally, the cementite will tend towards its equilibrium chemical composition when exposed to elevated temperatures for prolonged periods of time. This generally means that its substitutional solute content increases with time. It can be shown [20] that this change is given by:

$$t = \frac{\pi[x^\theta(\overline{c} - c^\theta)]^2}{16D_\alpha(c^{\alpha\theta} - \overline{c})^2} \tag{6}$$

where it is assumed that the particle is in the form of a thin plate of thickness x^θ, t is the time at the annealing temperature, c^θ is the average cementite (θ) composition at time t. D_α is the diffusion coefficient of the substitutional solute in ferrite, $c^{\alpha\theta}$ is the concentration in ferrite which is in equilibrium with cementite, and $\overline{c}$ is the starting composition of the carbide (Fig. 5b). Note that c^θ is not the concentration $c^{\theta\alpha}$ in cementite which is in *equilibrium* with ferrite. The diffusion flux in the ferrite is so small that the concentration in the cementite at the boundary cannot build up to the equilibrium level since any enrichment at the interface is relieved by diffusion within the cementite. This is because $(\overline{c} - c^{\alpha\theta})$ which drives the diffusion within the ferrite is much smaller than $(c^{\theta\alpha} - \overline{c})$, *i.e.* the solubility of elements such as chromium is much larger in cementite than in ferrite. It follows that in spite of the diffusion flows, the concentration distribution in the cementite is always likely to be quite uniform. This is a useful result since it makes it reasonable to determine the particle composition using microanalysis

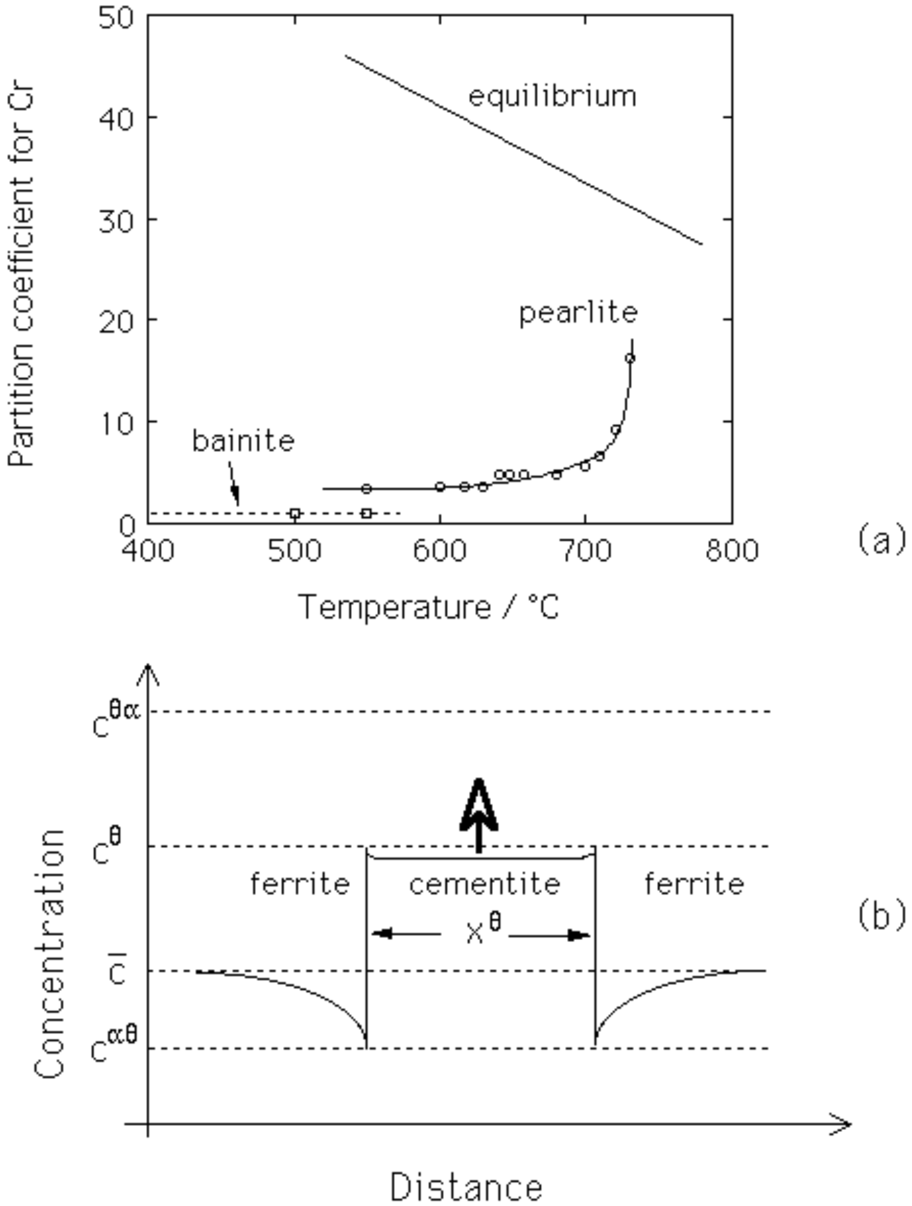

Fig. 5: (a) The partition coefficient for cementite in bainite and pearlite, together with equilibrium data [27]. The partition coefficient is the ratio of the concentration in cementite to that in the ferrite.(b) The concentration profile that develops during the enrichment of a cementite particle.

techniques which gather information from the entire particle. Thus the concentration in the cementite rises uniformly from $\overline{c}$ to $c^{\theta\alpha}$.

Equation 6 indicates that the change in composition $(c^{\theta} - \overline{c})$ should vary with $t^{\frac{1}{2}}$ during isothermal annealing; this is described as a *parabolic* law. This contrasts with the common assumption made even today, that the change should follow $t^{\frac{1}{3}}$ kinetics. It is often not possible in practice to distinguish between the two exponents; the experimental data give reasonable linear fits with either relationship. However, values of the diffusion coefficient extracted from such plots are only correct in the case for parabolic kinetics [28]. This confirms the physical significance of equation 6, which can extrapolated with more confidence than the $t^{1/3}$ relationship. An additional advantage is that the effect of the steel chemistry is explicitly included in equation 6 via the equilibrium and average compositions, so that data from many different alloys can be interpreted together.

Fig. 6 shows experimental measurements of the composition of cementite as a function of tempering time, for a microstructure which was initially fully bainitic [29,30]. The steel composition is Fe–0.1C–0.24Si–0.48Mn–0.84Cr–0.48Mo wt.%; the reason why the cementite composition is richer than the average is because a stress–relief heat treatment was given prior to ageing. There are a number of important features in this graph other than the fact that the parabolic law is verified. It is obvious that the largest changes are observed for chromium, which would therefore be a good element to monitor. This is because the solubility of Cr in the cementite is much larger than that of Mn or Mo (Table 4). Notice that the solubility varies with temperature, becoming smaller with increasing temperature.

	Equilibrium wt.%, 703 °C		Equilibrium wt.%, 550 °C	
	$c^{\alpha\theta}$	$c^{\theta\alpha}$	$c^{\alpha\theta}$	$c^{\theta\alpha}$
Cr	0.52	21.3	0.30	36.0
Mo	0.40	5.8	0.34	9.3
Mn	0.38	6.7	0.29	13.2

Table 4: Calculated equilibrium concentrations for Fe–0.1C–0.24Si–0.48Mn–0.84Cr–0.48Mo wt.% alloy used by Afrouz *et al.* These calculations are specific to this steel.

It should also be emphasized that the equilibria listed in Table 4 are steel specific and will vary greatly within the range of power plant alloys used typically in industry. A simple method for estimating the values is to write the partition coefficient for element Z as follows:

$$k_Z = \frac{c^{\theta\alpha}}{c^{\alpha\theta}} \simeq \exp\left\{\frac{A + BT}{RT}\right\} \tag{7}$$

where the parameters A and B are listed in Table 5 [31]. The partition coefficient only gives a ratio – to calculate the actual concentrations requires the following further relationship which derives from mass balance:

$$\overline{c} = c^{\theta\alpha}V_\theta + \frac{c^{\theta\alpha}}{k_Z} - \frac{c^{\theta\alpha}V_\theta}{k_Z} \tag{8}$$

V_θ can be estimated using the lever rule with carbon, so that the equilibrium compositions of the two phases can easily be calculated as a function of heat treatment and average composition.

Another feature highlighted by the parabolic law is the dependence of enrichment on the particle size x^θ. Smaller particles enrich faster and saturate earlier because they are smaller reservoirs for solute (Fig. 7).

The model described above predicts parabolic kinetics, which can be considered to have been verified by published experimental data. Although the data refer to time periods as long as 10,000 h, the time scales of interest are much larger, of the order of 260,000 h. Data can of course be obtained from steels which have been in service but they can be quite unreliable

Element Z	A / J mol^{-1}	B / J mol^{-1} K^{-1}
Cr	47028	-17.45
Mn	42844	-20.21
Mo	27363	-5.86
Ni	-2619	-2.80
Si	0	-25.10

Table 5: Compilation of parameters used for the calculation of partition coefficients [31].

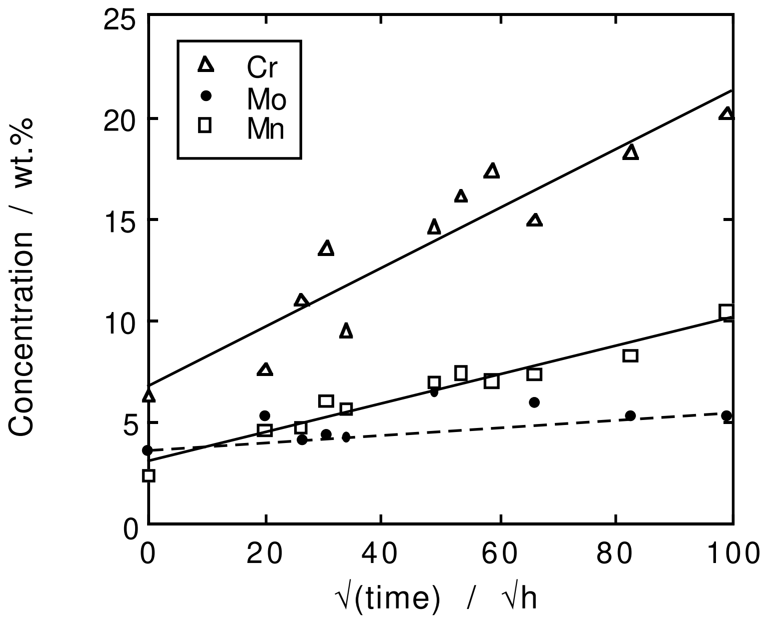

Fig. 6: Measured changes in the chemical composition of cementite particles as a function of the square root of time, during ageing at 550 $^\circ C$. The steel composition is Fe–0.1C–0.24Si–0.48Mn–0.84Cr–0.48Mo wt.%. It was heat treated to give a fully bainitic microstructure, stress–relieved at 730 $^\circ C$ for one hour and then tempered at 550 $^\circ C$ for the periods illustrated. Data from Afrouz, Collins and Pilkington [19].

because the history is then uncertain. It would not be safe to extrapolate the parabolic law to very long times, because the analytical expression does not account for a phenomenon known as *soft–impingement*. In this, the diffusion fields of adjacent particles begin to overlap and significantly interfere, slowing down the enrichment process until it stops completely when

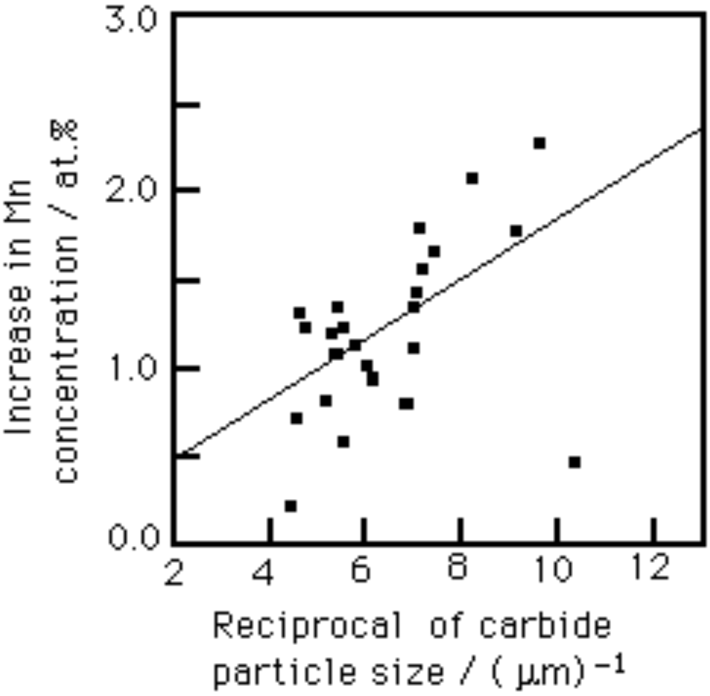

Fig. 7: Size dependence of cementite enrichment (annealed at 565 $^\circ C$ for 4 weeks [29,30].

equilibrium is achieved. Such a process cannot easily be treated analytically. Bhadeshia has used a finite difference method instead; some results are presented in Fig. 8, for precisely the experiments reported by Afrouz *et al.*. The parabolic law is a good approximation during the 'early' stages but the effect of soft–impingement is to cause deviations with a complete halt when the carbide saturates with the solute concerned. Manganese and molybdenum do so quite rapidly for this particular example. Thus, the numerical method (finite difference) can be used to extrapolate to very long times.

Pearlite

It has been emphasised that to ratio of substitutional solute to iron atom ratio is the same everywhere in a bainitic or martensitic microstructure as in the alloy as a whole. This is not the case for pearlite where the reconstructive mechanism of transformation ensures that the cementite is enriched with substitutional solutes, though often not to the extent expected from equilibrium. This makes it impossible to predict the initial composition of the cementite in pearlite. It turns out that for calculation purposes, this is not a serious problem for long ageing times, since the degree of enrichment then tends to be much larger than the starting solute level (Fig. 9).

Effect of Carbon

There are two effects which depend on the carbon concentration of the steel. The ternary Fe–Cr–C phase diagram on the $(Fe, X)_3C/\alpha$ field shows that an increase in the carbon concentration is accompanied by a decrease in the equilibrium concentration of chromium in the carbide. Thus, the carbide enrichment rate is expected to decrease. A further effect is that the volume fraction of cementite increases, in general leading to an increase in particle thickness and volume fraction. The thickness increase retards the rate of enrichment (equation 6). If

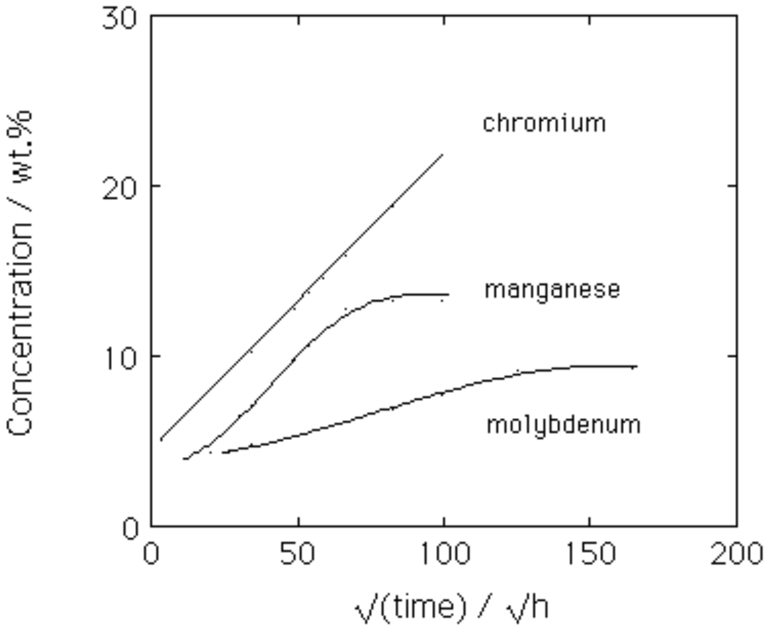

Fig. 8: Calculated changes in the chemical composition of cementite particles as a function of the square root of time, during ageing at 550 $^{\circ}C$. The steel composition is Fe–0.1C–0.24Si–0.48Mn–0.84Cr–0.48Mo wt.%. The calculations are done using a finite–difference method [20].

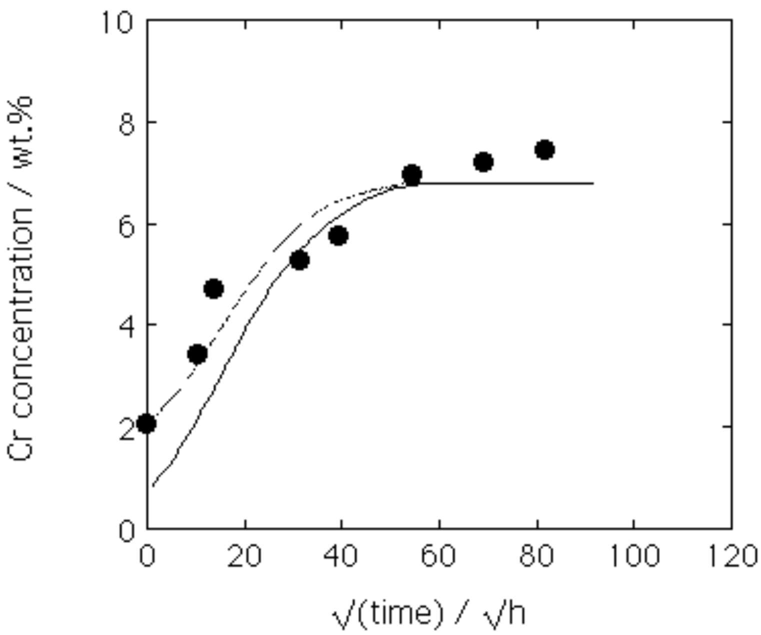

Fig. 9: Data for the enrichment of cementite associated with pearlite, and calculated curves assuming zero enrichment at $t = 0$ (continuous curve), and a finite enrichment at $t = 0$ (dotted line) [32].

the carbide particles are closer to each other then soft–impingement occurs at an earlier stage, giving a slower enrichment rate at the later stages of annealing.

Local variations in carbon concentration may have a similar effect to changes in average concentration. Such variations can be present through solidification induced segregation, or because of microstructure variations caused by differences in cooling rates in thick sections. It is well known that the microstructure near the component surface can be fully bainitic with the core containing a large amount of allotriomorphic ferrite in addition to bainite. In the latter case, the bainite which grows after the allotriomorphic ferrite, transforms from high carbon austenite. The associated carbides are then found to enrich at a slower rate (Fig. 10a). This discussion emphasises the role of carbon, an element which unfortunately is not tightly specified in creep resistant alloys.

High–Alloy Steels, Alloy Carbides

The vast majority of steels used in the power generation industry have a total alloy concentration less than 5 wt.%, but there are richer martensitic alloys such as the 9Cr1Mo, 12Cr1MoV destined for more stringent operating conditions. For low alloy steels, the initial carbide phase found immediately after the stress–relief heat treatment (typically several hours at 700 °C) is cementite. The cementite is very slow to enrich and to convert to alloy carbides, thus allowing the process to be followed over a period of many years during service. As the concentration of carbide forming elements is raised, the kinetics of cementite enrichment and alloy carbide precipitation become more rapid (Fig. 10b). Thus, relatively stable alloy carbides tend to dominate the microstructure after short periods in service or even after the stress relief heat treatment [33]. The alloy carbides form with virtually their equilibrium compositions, and hence show no change on annealing. Fig. 11 shows microanalysis data from vanadium–rich carbides for two samples with average composition

Fe-0.11C-0.3Mn-0.28Mo-0.23V-0.023N wt.%

The "virgin" sample was produced by tempering at 700 °C for an unspecified time period, following normalisation at 950 °C for an unspecified period. The exposed sample had in addition spent 10^5 hours at 540 °C and 50 MPa. It is clear that there is no significant difference between the carbide compositions from the two samples. There is therefore little prospect of estimating the remaining life of high alloy steels, or of steels in general, by following changes in the chemical compositions of alloy carbides. As a matter of interest, Fig. 11b shows the chromium and molybdenum concentrations of the most prominent alloy carbide found in most power plant steels (see also Tables 2,3).

One possibility is to follow the detailed microstructural changes. Fig. 12 is a simplified presentation of the evolution of carbide and Laves phases during the ageing of a 9CrMoVW steel *(NF616)* which is tempered from its martensitic state at a temperature of 600 °C over six orders of magnitude of time. Obviously, an identification of the fractions of the phases could help to fix the state of the steel. Some of the precipitation reactions are sensitive to temperature. For example, the driving force for the precipitation of Laves phases decreases greatly as the temperature increases.

CAVITATION DAMAGE

Deformation by creep is far from homogeneous on a microstructural scale. One manifestation of this is the formation of cavities at the grain boundaries between differently oriented crystals. Cavitation plays a critical role in the events leading to ultimate failure and hence is a direct measure of remaining life.

The cavities tend to form on boundaries with normals parallel to the principal tensile stress, by a process of nucleation and growth. Thus, at any instant of life, only a fraction of the

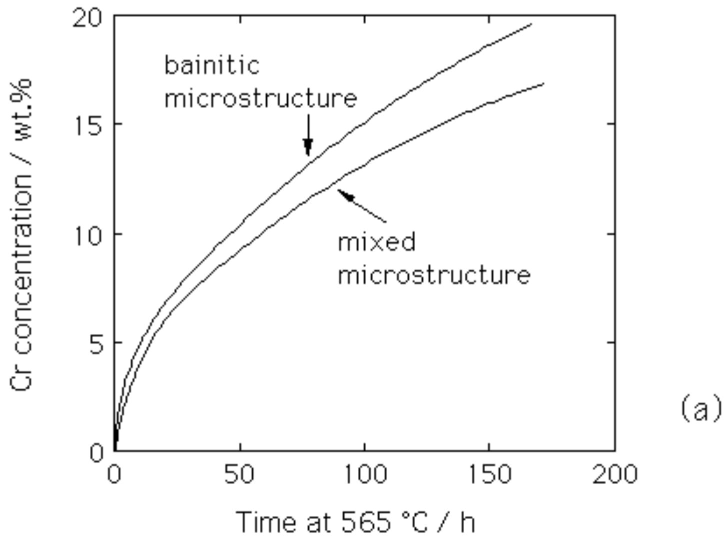

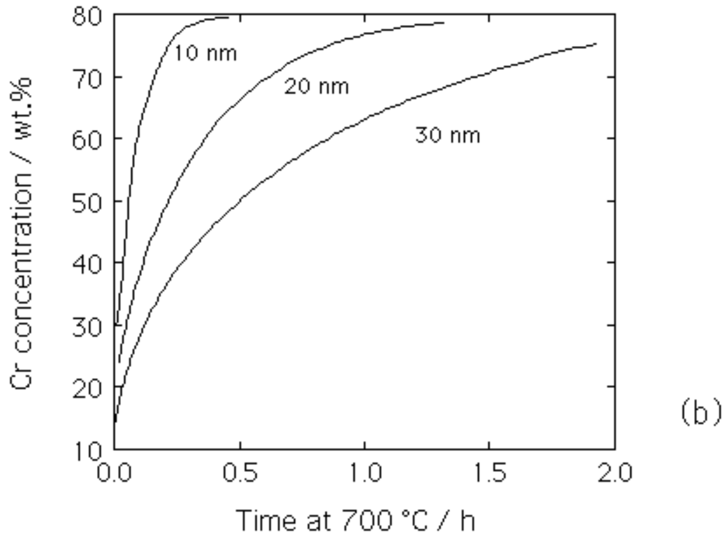

Fig. 10: (a) $2\frac{1}{4}$Cr1Mo steel, cementite enrichment in a fully bainitic microstructure and one which is a mixture of allotriomorphic ferrite and bainite [29,30]. (b) Rapid saturation of cementite in a 12Cr1MoV steel aged at 700 $^\circ C$, as calculated for a variety of particle sizes [33].

transverse boundaries have cavitation damage. There are constraints to cavity formation when only some of the transverse boundaries are cavitated, and this has important consequences on the creep rupture life [35]. In Fig. 13a, all the transverse boundaries have identical cavities. The regularity of the structure allows the cavities to grow unconstrained, the extension along the stress axis being accommodated by grain boundary sliding. This is not the case when, as illustrated in Fig. 13b, only some of the boundaries have cavities. The extension due to the cavities at wx results in sliding which causes the adjacent grains to overlap at yz. This matter in the shaded region at yz must be carried away by diffusion before the cavities at wx can continue to grow. This in effect imposes a constraint on the growth of the cavities when compared with the situation in Fig. 13a. The physical basis of the retardation is that cavity

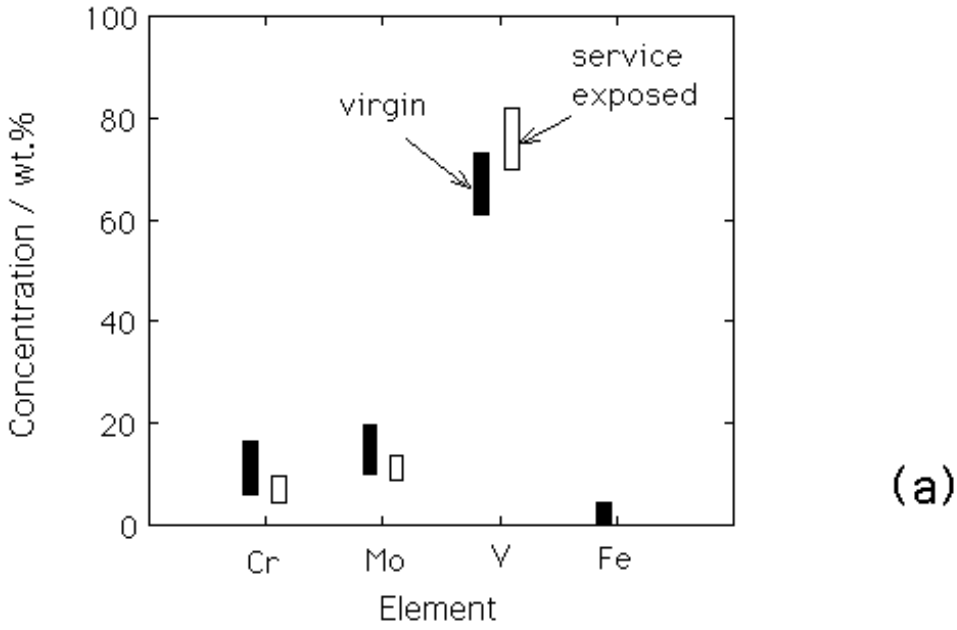

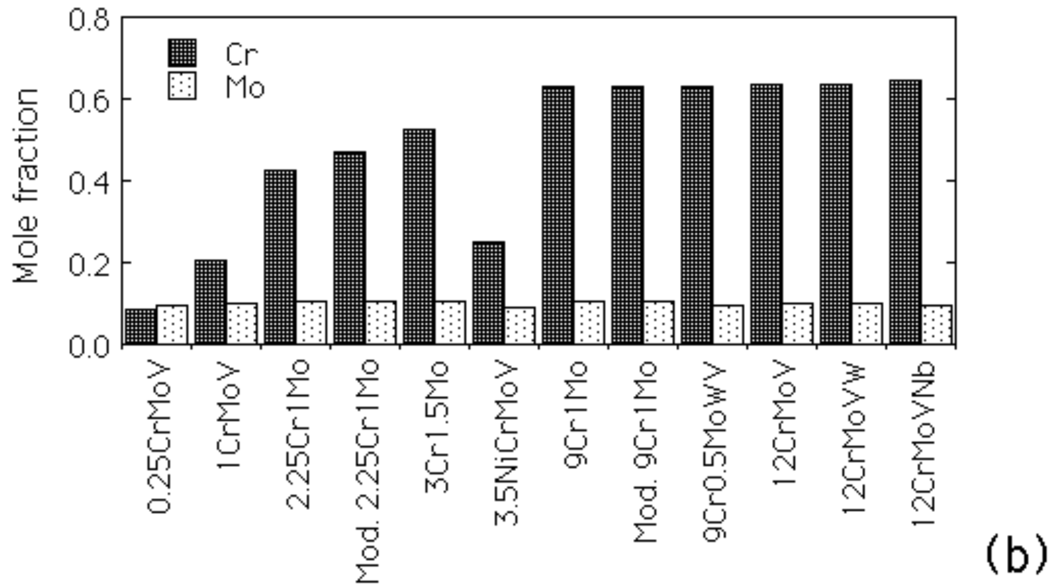

Fig. 11: (a) The chemical compositions of vanadium–rich carbides in virgin material and in samples which had been in service for ten years [22]. (b) The concentrations of Cr and Mo in $M_{23}C_6$ in the power plant steels listed in Table 2, for 565 $°C$. The data are calculated using the *MTDATA* program.

growth now becomes controlled by the rate of matrix creep. The retardation is very significant, as seen in Fig. 13c.

The cavitation is characterised by an 'A–parameter' determined as the number fraction of cavitated grain boundaries traversed by a scan parallel to the stress axis of a creep test

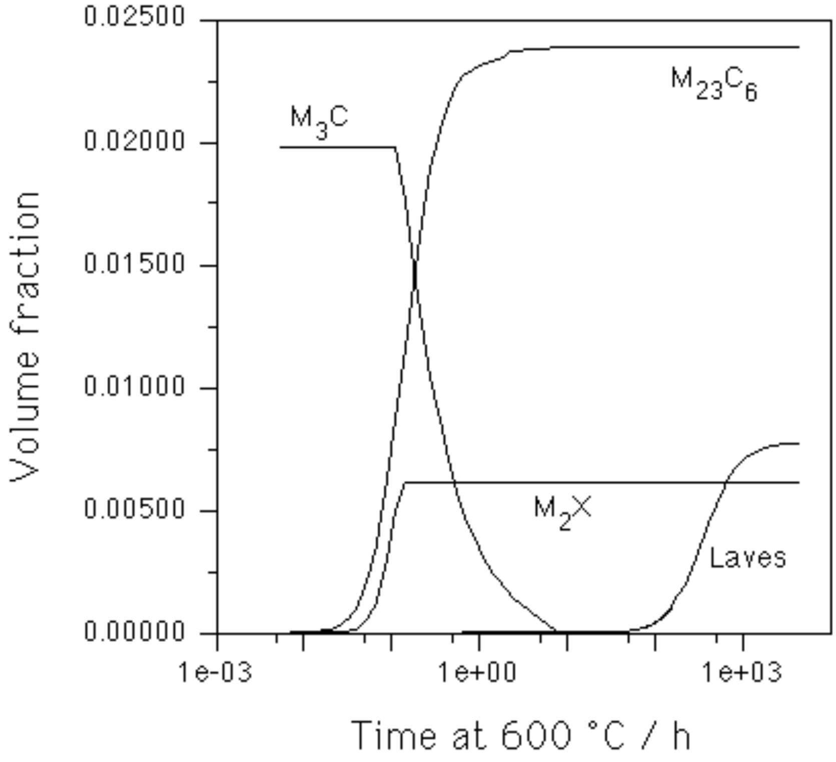

Fig. 12: Calculated evolution of the phase fractions in a 9CrMoVW steel (*NF616*) during tempering at 600 $^\circ C$ [34].

specimen, whilst avoiding the necked region [36]. There is considerable work in the published literature dealing with the kinetics of the constrained growth of cavities growth [1] and this has been used to express the parameter A as follows:

$$A = 1 - \left(1 - \frac{t}{t_r}\right)^{n(1-\frac{\epsilon}{\epsilon_r})} \tag{9}$$

where t is the time, t_r the time to rupture, ϵ the creep strain, ϵ_r the creep rupture strain and n a fitted constant. Fig. 14 shows both experimental data and a curve calculated using equation 9 and assumed values of $\epsilon_r/\epsilon = 2.5$ and $n = 3$ [36]. The data seem follow the form indicated by the equation but there are other results [12,37] which suggest that the relationship remains linear up to the point of life–exhaustion, although the degree of scatter in the A–parameter increases significantly for a life fractions greater than 0.96.

The A–parameter is defined in terms of the number of transverse boundaries which are cavitated. Many models for creep associate fracture with a complete loss of area available to support the load as the cavities coalesce along the appropriate plane [7,38,39]. A strict measure of the damage would then be *area* of transverse boundaries that is decorated by cavities. The A–parameter on the other hand could reached unity before the transverse boundaries are completely detached. However, this may not be a problem in practice if the rate of damage increase in the final stages is very high.

Another method of assessing the remaining life using cavitation damage involves the measurement of the number density of cavities, which seems to relate directly to the creep strain during uniaxial loading [6]. This may not in fact amount to a different method (compared

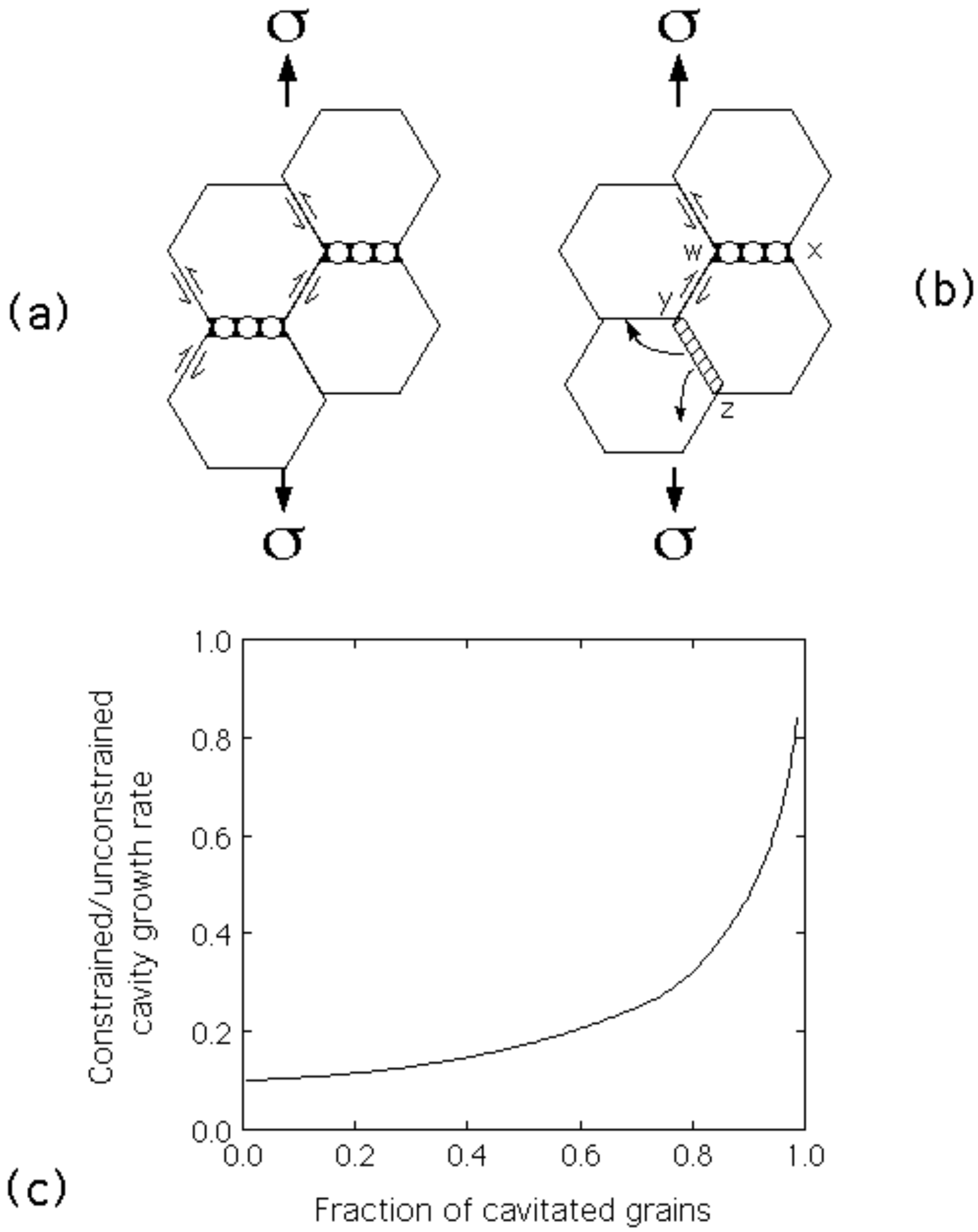

Fig. 13: The effect of constraint on the growth rate of cavities. (a) All transverse boundaries cavitated. (b) Non–uniform cavitation. (c) The reduced cavity growth rate when cavitation is not uniform [35].

with the A–parameter) in the context of steels where the important cavities tend to form at the grain boundaries.

The volume fraction of cavities increases approximately with the strain and can be used as a measure of remaining life [7], although differences in the distribution of cavities (due to differences in microstructure) could introduce variations in creep life at constant cavity

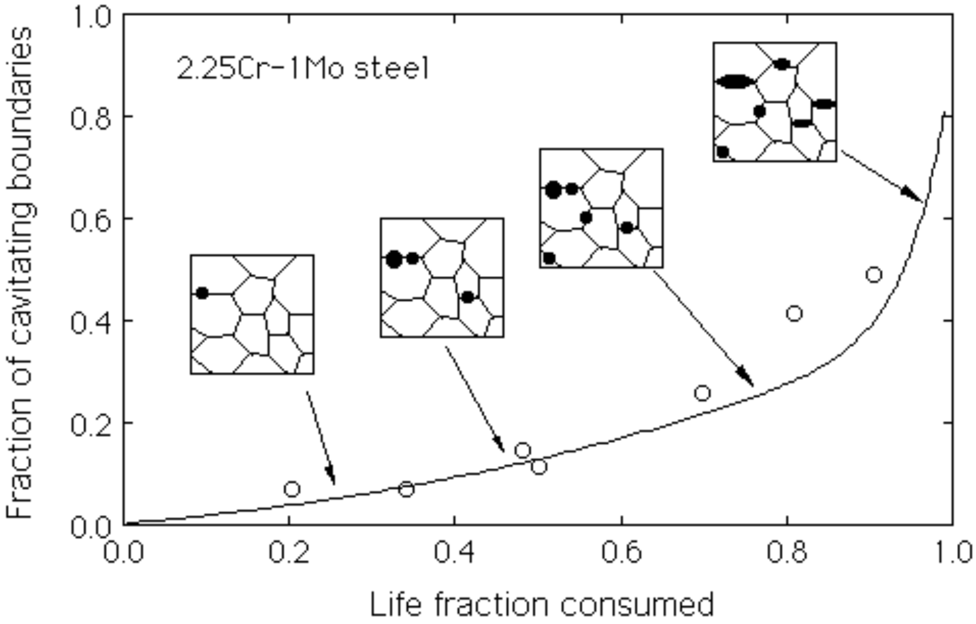

Fig. 14: The fraction of cavitating grain boundaries as a function of the life fraction consumed [36].

fraction.

FRACTURE TOUGHNESS

It is well established that the fracture toughness of many power plant steels deteriorates during service for two reasons. Firstly, the carbide particles, particularly those located at boundaries, coarsen and hence provide easier sites for crack or void nucleation. Secondly, the segregation of impurities to interfaces has an opportunity to proceed to its equilibrium extent during service. This tendency to embrittle during service is sometimes simulated by an accelerated step cooling experiment in which the sample is held at a variety of decreasing temperatures over the embrittlement range, and then allowed to cool to ambient temperature at a very slow rate. Unfortunately, although the procedure does allow the sensitivity of the sample to embrittlement phenomena to be tested, the data cannot be used to discover the state of the steel in its ageing process (a remaining life assessment).

Fig. 15a shows how the fracture assessed impact transition temperature (FATT) varies with the mean carbide particle size in a $2\frac{1}{4}$Cr1Mo steel [8]. Fig. 15b shows the complete transition curves for both the virgin steel (*i.e.* at implementation into service) and for an ex–service sample which had experienced 88,000 h at 813 K. The points represent samples of virgin steel subjected to 873 K for 10,000 h in an attempt to simulate prolonged service at 813 K. These conditions were chosen in order to achieved the same Larson–Miller parameters for the ex–service and simulated samples. It is clear that the agreement between the simulation and service exposed steel is excellent, allowing the method to be added to the panoply of tools available for remaining life assessment.

CONCLUSIONS

The present work, which is limited by deadlines, is by no means a comprehensive review of the

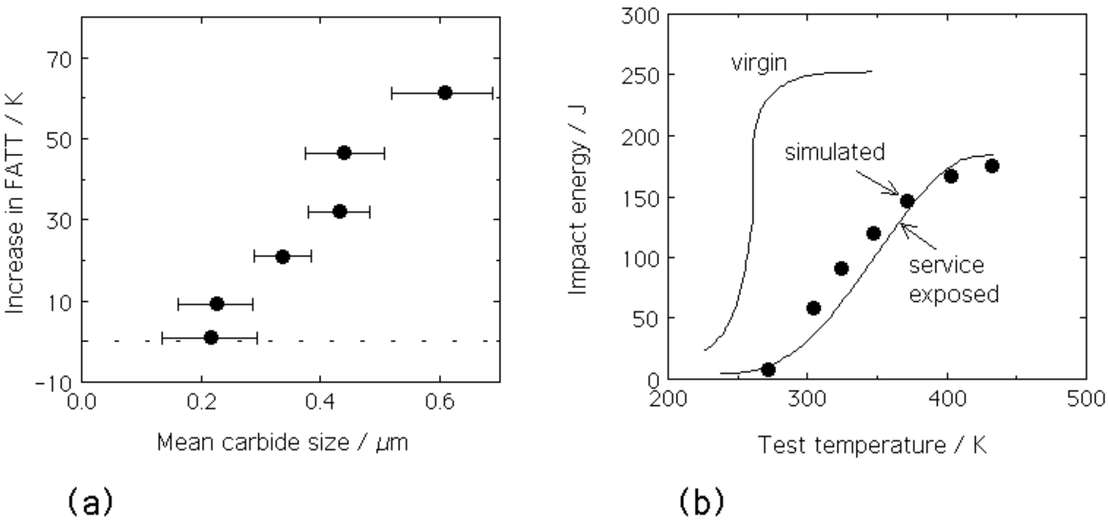

Fig. 15: Impact test data on $2\frac{1}{4}$Cr1Mo steel. (a) Change in the fracture assessed impact transition temperature with the mean carbide size as a function of ageing. (b) Comparison of the impact energies of the steel in its virgin condition, after service exposure at 813 K for 88,000 h and for a service–simulated sample (873 K for 10,000 h). After Wignarajah *et al.* [8].

available literature. But it should be obvious that there is a vast array of methods available for the assessment of remaining life in power plant steels. Impressive as the methods are, they must be used with experience and caution since the number of variables (and indeed the variability) is quite large.

ACKNOWLEDGMENTS

It is a pleasure to acknowledge David Gooch (National Power plc.), the late Brian Greenwell (NEI Parsons), and Roger Conroy (NEI Parsons) for their generous support of our research over a period of more than eleven years. I am also grateful to the Royal Society for a Leverhulme Trust Senior Research Fellowship and to Professor Alan Windle for the provision of laboratory facilities at the University of Cambridge.

REFERENCES

1. H. E. Evans: *Mechanisms of Creep Fracture,* Elsevier Applied Science Publishers, Essex, England (1984)
2. T. Goto: *Creep and fracture of engineering materials and structures,* Swansea, Pineridge Press, (1984) 1135.
3. B. J. Cane and J. A. Williams: *International Materials Reviews* **32** (1987) 241–262.
4. M. C. Askins and K. Menzies: *Unpublished work,* referred to in Gooch and Townsend, 1987 (1985)
5. D. J. Gooch, M. S. Shammas, M. C. Coleman, S. J. Brett and R. A. Stevens: *Proc. Conf. Fossil Power Plant Rehabillitation, Cincinnati, Ohio,* ASM International, Ohio (1989) Paper 8901-004.
6. B. F. Dyson and D. McLean: *Metal Science* **6** (1972) 220.
7. G. K. Walker and H. E. Evans: *Metal Science* **4** (1970) 155.
8. S. Wignarajah, I. Masumoto and T. Hara: *ISIJ international* **30** (1990) 58–63.
9. E. L. Robinson: *Trans. Am. Soc. Mech. Engrs.* **74** (1952) 777.
10. B. J. Cane and R. D. Townsend: *CEGB report TPRD/L/2674/N84,* Leatherhead, Surrey (1984)

11. B. W. Roberts and A. Strang: *Refurbishment and Life Extension of Steam Plant,* Institution of Mechanical Engineers, London (1987) 205–213.
12. J. Maguire and D. J. Gooch: *Proc. Int. Conf. Life Assessment and Extension,* The Hague, (1988)
13. A. J. Tack, J. M. Brear and F. J. Seco: *Creep: Characterisation, Damage and Life Assessment,* eds D. A. Woodford, C. H. A. Townley and M. Ohnami, ASM International, Ohio, U.S.A. (1992) 609–616.
14. P. Battaini, D. D'Angelo, G. Marino and J. Hald: *Creep and Fracture of Engineering Materials and Structures,* Institute of Metals, London (1990) 1039–1054.
15. S. D. Mann, D. G. McCulloch and B. C. Muddle: *Metallurgical and Materials Transactions A* **26A** (1995) 509–520.
16. R. B. Carruthers and M. J. Collins: *CEGB Report NER/SSD/M/80/327* (1980) .
17. R. B. Carruthers and M. J. Collins: *Quantitative microanalysis with high spatial resolution,* Metals Society, London (1981) 108–111.
18. R. B. Carruthers and M. J. Collins: *Metal Science* **17** (1983) 107.
19. A. Afrouz, M. J. Collins and R. Pilkington: *Metal Technology* **10** (1983) 461.
20. H. K. D. H. Bhadeshia: *Materials Science and Technology* **5** (1989) 131–137.
21. B. J. Cane and J. A. Williams: *International Mat. Rev.* **32** (1987) 241–262.
22. R. Singh and S. Banerjee: *Scripta Metallurgica et Materialia* **24** (1990) 1093–1098.
23. S. D. Mann and B. C. Muddle: *Microstructures and Mechanical Properties of Aging Material,* eds P. K. Liaw, R. Viswanathan, K. L. Murty, E. P. Simonen and D. Frear, The Minerals, Metals and Materials Society, Warrendale, Pennsylvania (1993) 301–308.
24. S. D. Mann and B. C. Muddle: *Microstructures and Mechanical Properties of Aging Material,* eds P. K. Liaw, R. Viswanathan, K. L. Murty, E. P. Simonen and D. Frear, The Minerals, Metals and Materials Society, Warrendale, Pennsylvania (1993) 309–317.
25. S. D. Mann and B. C. Muddle: *Micron* **25** (1994) 499–503.
26. H. K. D. H. Bhadeshia: *Mathematical Modelling of Weld Phenomena 2,* eds H. Cerjak and H. K. D. H. Bhadeshia, Institute of Materials, London (1995) 71–118.
27. J. Chance and N. Ridley: *Metallurgical Transactions A* **21A** (1981) 1205–1213.
28. P. Wilson: *Ph. D. Thesis,* University of Cambridge (1991) .
29. R. C. Thomson and H. K. D. H. Bhadeshia: *Materials Science and Technology* **10** (1994) 193–204.
30. R. C. Thomson and H. K. D. H. Bhadeshia: *Materials Science and Technology* **10** (1994) 205–208.
31. D. Venugopalan and J. S. Kirkaldy: *Hardenability concepts with applications to steels,* eds D. V. Doane and J. S. Kirkaldy, AIME, Warrendale, Pennsylvania (1978) 249–268.
32. X. Du, R. C. Thomson, J. Whiteman and H. K. D. H. Bhadeshia: *Materials Science and Engineering A* **A155** (1992) 197–205.
33. R. C. Thomson and H. K. D. H. Bhadeshia: *Metall. Trans. A* **23A** (1992) 1171–1179.
34. J. D. Robson and H. K. D. H. Bhadeshia: *Creep Resistant Metallic Materials,* published by Vitkovice, Czech Republic (1996) 83–91.
35. B. F. Dyson: *Metal Science* **10** (1976) 349–353.
36. M. S. Shammas: *Unpublished work,* referred to in Gooch and Townsend, 1987 (1985)
37. M. S. Shammas: *Refurbishment and Life Extension of Steam Plant,* Inst. Mechanical Engineering, London (1987) 289–295.
38. D. Hull and D. E. Rimmer: *Philosophical Magazine* **4** (1953) 673.
39. R. Raj and M. F. Ashby: *Acta Metallurgica* **23** (1975) 653.